On-chip differential interference contrast (DIC) phase imager and beam profiler based on Young's interference

Xiquan Cui, Matthew Lew, Xin Heng, Changhuei Yang

Xiquan Cui, Matthew Lew, Xin Heng, Changhuei Yang, "On-chip differential interference contrast (DIC) phase imager and beam profiler based on Young's interference," Proc. SPIE 6441, Imaging, Manipulation, and Analysis of Biomolecules, Cells, and Tissues V, 64411F (19 February 2007); doi: 10.1117/12.699920

SPIE.

Event: SPIE BiOS, 2007, San Jose, California, United States

On-chip differential interference contrast (DIC) phase imager and beam profiler based on Young's interference

Xiquan Cui[1*], Matthew Lew[1], Xin Heng[1], Changhuei Yang[1]
[1]Electrical Engineering, California Institute of Technology, Pasadena, CA, 91125;

ABSTRACT

In this article, we will present a novel differential interference contrast (DIC) phase imaging device based on Young's interference. It is mainly based on either two or four nano apertures defined in an optically opaque aluminum film on a CMOS imaging sensor chip. It provides linear and disentangled differential phase and intensity images simultaneously. Furthermore, it's simple, free of bulky optical elements and compatible to the planar micro fabrication process. All of these features make it a promising device for the on-chip high resolution DIC phase imaging and beam profiling. The fabrication and operation of the device is explained in details. The performance is evaluated theoretically and is verified experimentally by examining the phase and intensity profile of a Gaussian beam and an optical vortex. The 2D quantitive differential phase distribution of an optical vortex has been recorded directly by our device with 1μm resolution.

Keywords: Optofluidics, Biophotonics, Nanophotonics, Microfluidics, Differential interference contrast microscopy, Beam profiler.

1. Introduction

Optofluidic Microscopy (OFM) is a new microscope imaging concept developed in our group[1,2]. We create microscopes on a chip. The operating principle of OFM is very simple. We coat a linear CCD imaging sensor with a thin metal film, and punch a slanted line of equal spaced nano apertures. On top of the linear CCD, we stack a PDMS microfluidic channel. So when we flow cells or microorganisms through the microfluidic channel, each CCD pixel will record a different line profile of the transmission image of the biological sample through the nano apertures. By stacking the line traces together appropriately, we can form an image of the object. There are no bulky optical elements in OFM. So it can be directly integrated into a microfluidic network compactly and cheaply, which makes OFM a promising component for the on-chip imaging in a microfluidic system. The resolution of OFM is only limited by the size of nano aperture. So it has the potential to achieve super-resolution. Right now besides the research on the compact[3] and high-resolution[4] versions of OFM, we are also thinking of adding more functionality to the OFM family, for example fluorescence detection and phase imaging. In this paper, we will present a novel DIC phase imaging device based on Young's interference. It can be adapted for the phase imaging capability of OFM.

Nowadays there are two main types of phase imaging techniques. One is based on wavefront sensor; the other is based on interferometer system. Shack-Hartmann[5] is a typical wavefront sensor based system. It uses an array of microlenses to subdivide the wavefront and translate the local slopes of the wavefront into the positions of the focal spots on a 2D imaging sensor. It is widely used in astronomy and vision correction. But it has the disadvantages of being bulky, expensive, and low lateral resolution (~100μm). Conventional DIC microscope[6] is an interferometer based system. It takes two images of the sample, displaces them slightly, and let them interfere. Because it renders DIC images of high contrast for the biology samples, it is widely used by biologists and doctors. But it requires expensive and bulky optical components. Furthermore, the DIC image contains entangled intensity and phase information, and the differential phase response is nonlinear too. So the conventional DIC microscopes are mainly used for qualitative phase imaging.

* Email: xiquan@caltech.edu

Imaging, Manipulation, and Analysis of Biomolecules, Cells, and Tissues V,
edited by Daniel L. Farkas, Robert C. Leif, Dan V. Nicolau, Proc. of SPIE
Vol. 6441, 64411F, (2007) · 1605-7422/07/$18 · doi: 10.1117/12.699920

In our DIC phase imaging device, two nano apertures are defined in an optically opaque aluminum film over a CMOS imaging sensor chip. The two nano apertures are used to select the sample beam and reference beam from the light field transmitted through the biological sample. Depending on the light path difference between them, the Young's interference pattern formed behind the two nano apertures will be centered at different positions on the CMOS sensor array. From the position of the center of the interference pattern, the differential phase information of the specimen can be achieved. At the same time, the total signal of the interference pattern gives the intensity information of the specimen. Since the intensity and phase response of our device is linear too, it is suitable for quantitive wavefront imaging. The lateral resolution of our DIC phase imaging device is only limited by the spacing between the two nano apertures. So super-resolution phase imaging could be achieved by simply reducing the spacing between the two nano apertures in our device. In addition, our device is based on a very simple Young's interference configuration, free of expensive and bulky optical components, and suitable for microfabrication. So it is a promising device for the on-chip high resolution DIC phase imaging and beam profiling.

In this manuscript, the fabrication and operation of the device is explained in details. The performance is evaluated theoretically and is verified experimentally by examining the phase and intensity profile of a Gaussian beam and an optical vortex. The 2D quantitive differential phase distribution of the optical vortex has been recorded directly by our device with 1μm resolution.

2. Method

The DIC phase imaging device is fabricated on a MT9V403 CMOS imaging sensor (Figure 1) from Micron Technology, Inc. The pixel size is 9.9μm×9.9μm. The pixel resolution is 640×480. On top of the CMOS sensor, we spin a 120μm thick SU8 photoresist as a spacer. Then a 200nm thick aluminum thin film is coated on top of the SU8 spacer by thermal evaporation as an optically opaque mask for the CMOS pixels. A FEI dual beam focus ion beam machine (NOVA 200) is used to punch nano apertures through the aluminum film at the center of the CMOS chip. The nano apertures are 500nm in diameter with 1μm spacing.

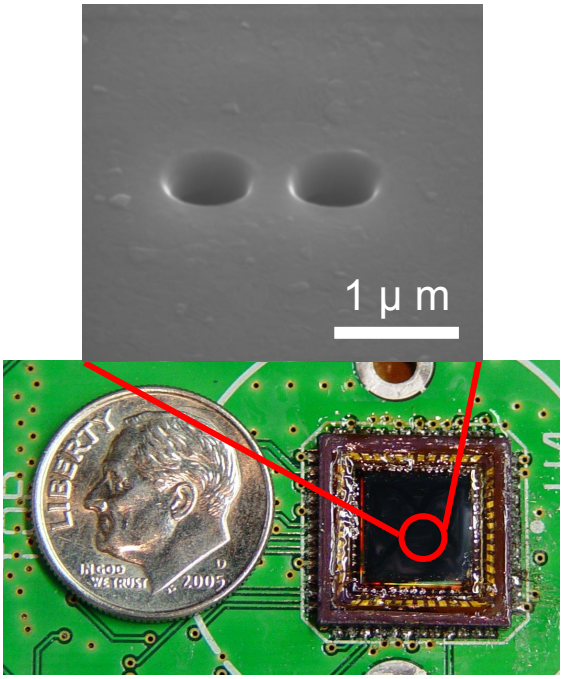

Figure 1: Two nano apertures punched on the aluminum film at the center of a CMOS chip by the focus ion beam machine.

Figure 2 provides an overview of the DIC phase imaging device. If we put a uniform specimen on top of the two nano apertures, the specimen won't change the flat wavefront of the plane wave illumination. The light beams exiting from the two nano apertures will carry the same phase. The two light beams interfere with each other and form the center lobe of the interference fringes right at the center of the CMOS sensor. If the sample is not uniform, the specimen will introduce a phase difference between the light beams shining onto the two nano apertures. When the lights exit from the two nano apertures, the central lobe of their interference pattern will shift to one side.

Assuming the location of the central lobe is x away from the center of the CMOS sensor, the spacing between the nano apertures is a, and distance from the nano apertures to the CMOS sensor is D, we can easily figure out the phase difference $\Delta\Phi$ introduced by the specimen with the simple Young's interference formula.

$$\Delta\phi \approx \frac{2\pi}{\lambda}\frac{a}{D}x \tag{1}$$

From Eq. (1), we can see the differential phase is linearly proportional to the location of the center lobe of the Young's interference pattern. The location of the center lobe can be easily predicted by the data of the interference pattern recorded by the CMOS sensor. If we integrate the signal of the whole interference pattern, it will give us the transmission of light through the specimen.

If we consider the light beam through one nano aperture as sample beam and the light beam through the other nano aperture as reference beam, we are actually doing shearing interference between the sample and reference beams, just as in the conventional DIC microscope. But our device has several advantages over the conventional DIC microscope. First, the differential phase response of our device is linear with respect to the location of the center lobe recorded by our device. Secondly, the differential phase and intensity information of the specimen are recorded by our device separately from the location of the center lobe and the total signal of the whole interference pattern respectively, which provides disentangled differential phase and intensity information of the specimen at the same time. Thirdly, the lateral DIC resolution of our device is only limited by the spacing between the two nano apertures. So super-resolution phase imaging could be achieved by simply reducing the spacing between the two nano apertures in our device. Furthermore, it's base on a very simple Young's interference configuration, free of expensive and bulky optical elements and suitable for the planar micro fabrication process. All of these features make it a promising device for the on-chip high resolution DIC phase imaging and beam profiling.

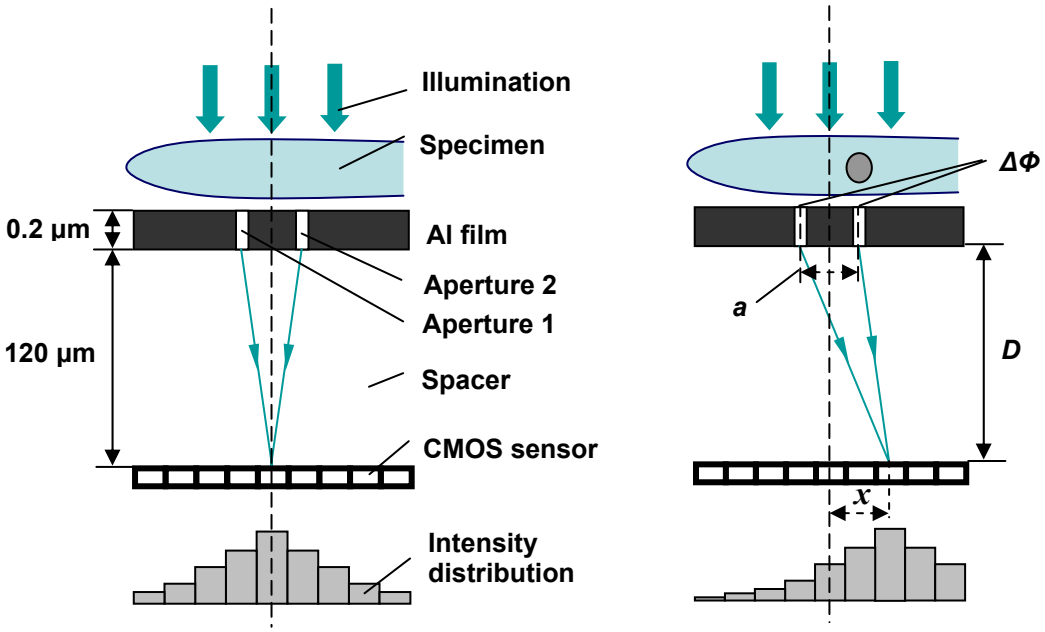

Figure 2: Operating principle of the DIC phase imaging device.

3. Characterization

In order to characterize the experimental differential phase responsitivity of our device, we illuminate a plane wave onto our device. By changing the incident angle of the plane illumination, we can introduce any phase difference between these two nano apertures. The actual phase difference can be calculated by the incident angle of the plane illumination and the spacing between the two nano apertures. The location of the center lobe of the interference pattern in our device changes with the incident angle of the plane illumination. In our experiment, we use the Gaussian fitting toolkit in Matlab to predict the location of the center lobe. Figure 3 shows the differential phase responsitivity curve of our DIC phase imaging prototype device. The figure shows good linear relationship between the differential phase and the location of the center lobe. The responsitivity is approximately 0.15μm/deg. The variation of the data could be due to the uncertainty of determining the incident angle of the plane illumination. In our prototype device, usually the center lobe of the interference pattern covers six CMOS pixels. With considering 8-bit quantization error, we did Monte Carlo simulation to determine the sensitivity of our prototype device. Within 1000 experiments, we still can easily distinguish 1 degree differential phase difference.

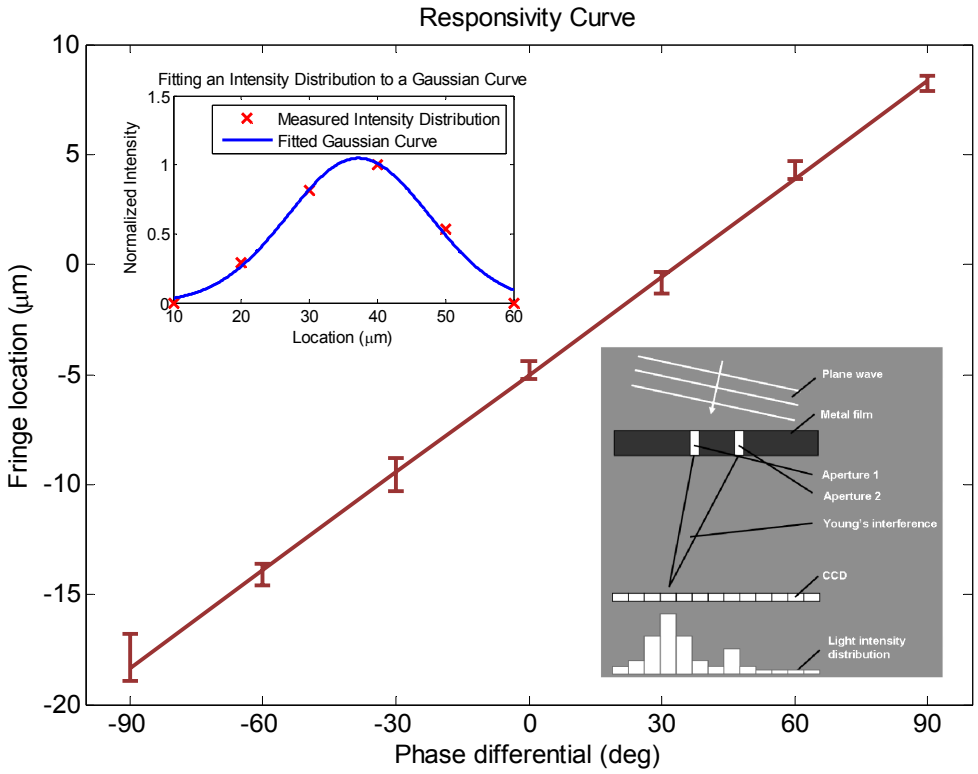

Figure 3: The characterization of the differential phase responsitivity of the DIC phase imaging prototype device.

4. Experimental results

4.1 Single axis DIC

In order to show the DIC imaging capability of our device, we used our device to profile the wavefront of the well known Gaussian beam. Since the two nano apertures in our prototype device only can measure the differential phase along the two nano apertures axis, we call this prototype device single axis DIC device. We coupled light from a 635 nm laser source (Thorlabs S1FC635) into Corning Puremode HI 780-5/125 single mode fiber to filter out the high order modes. Output light from the optical fiber was collimated by a lens with an 11 mm focal length (Thorlabs C220TM-B). On top of our DIC device, we used another Thorlabs C220TM-B lens to focus the laser beam onto the two nano apertures. Then we raster-scaned our device across different crosssections of the convergent Gaussian beam to sample the differential phase on each point (Figure 4(a)). The 2D raster-scan was driven by two Newport CMA-25CCCL linear actuators. Figure 4 (b), (c) and (d) show DIC images of the Gaussian beam at the converging, waist, and diverging regions respectively. In the converging and diverging regions, the differential phase changes from the negative values to the positive values, which is consistent with the phase change across the curved wavefront. In the waist region, the differential phase is almost a constant zero, which corresponds to the flat wavefront. We also integrated the differential phase to reconstruct the phase images of the Gaussian beam. Figure 4 (e), (f) and (g) show the reconstructed phase images of the Gaussian beam at the converging, waist, and diverging regions respectively. The curvatures of the converging, flat and diverging wavefronts are shown explicitly.

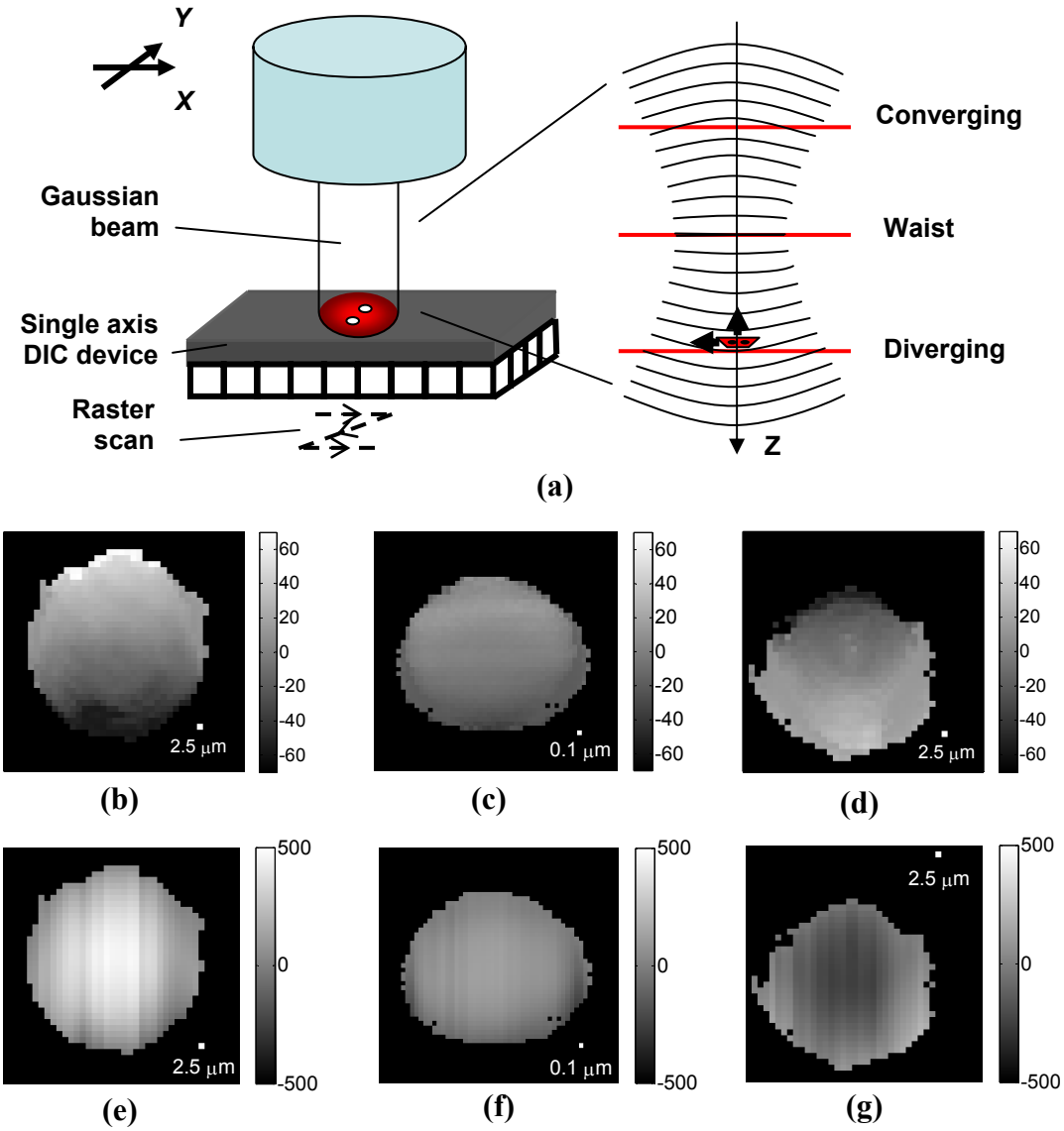

Figure 4: (a) Single axis beam profiling setup for a Gaussian beam. DIC images of a Gaussian beam at the (b) converging, (c) waist, and (d) diverging regions. Reconstructed phase images of the Gaussian beam at the (e) converging, (f) waist, and (g) diverging regions.

4.2 Double axes DIC

4.2.1 Four nano apertures configuration

The differential phase for a 2D phase distribution is usually a 2D vector field. So a natural evolution of the single axis DIC device is double axes DIC device. We simply punch a four apertures pair on the prototype device instead (Figure 5 (a), (b)). The aperture size is still 500nm. The spacings between two apertures in the X and Y axes are all 1μm. Simulations (Figrue 5 (c), (d), (e)) show that the center lobe of the four apertures interference pattern changes its location in the X and Y directions according to the phase difference in X and Y directions respectively and separately, as if it's two single axis devices working simultaneously.

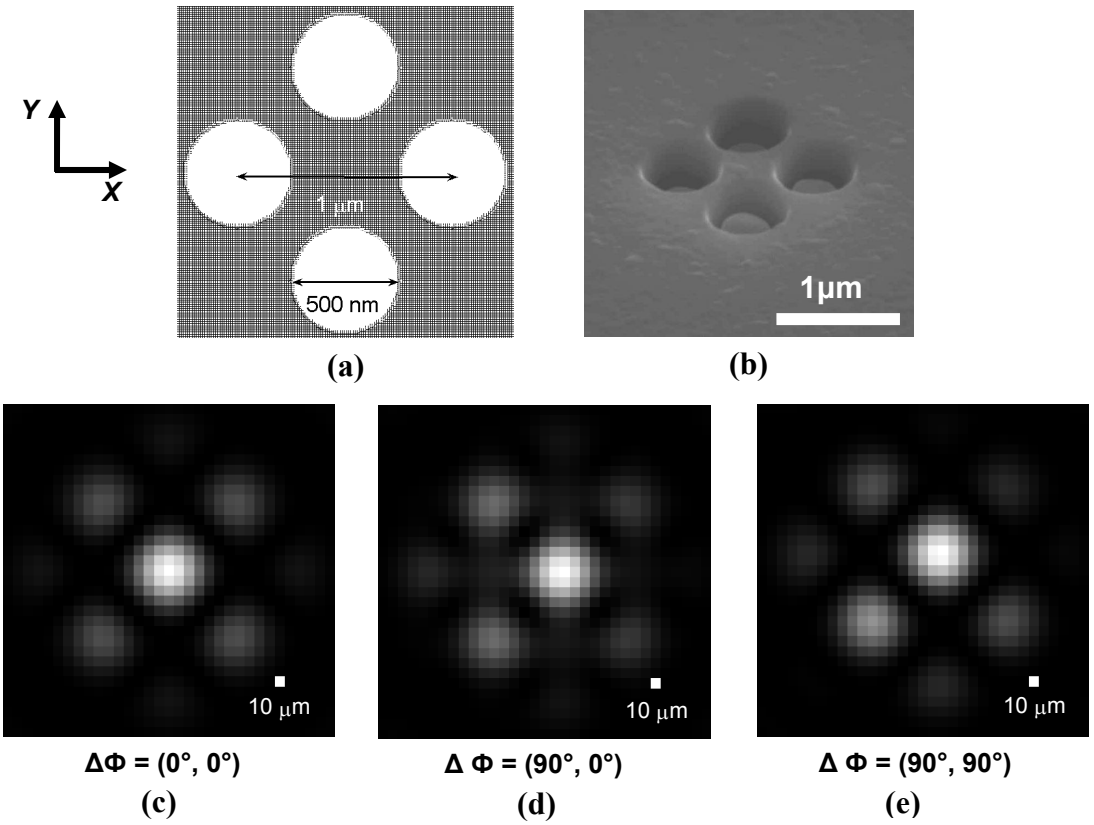

Figure 5: (a) Configuration of the four nano apertures in the double axes DIC device. (b) 30 degree tilt SEM image of the four nano apertures structure. The interference pattern of the four nano apertures when the differential phase in X and Y directions are (c) $\Delta\Phi = (0°, 0°)$, (d) $\Delta\Phi = (90°, 0°)$ and (e) $\Delta\Phi = (90°, 90°)$ respectively.

4.2.1 2D differential phase profiling of the optical vortex

In order to show the 2D differential phase vector imaging capability, we did 2D differential phase profiling of an optical vortex in a first order Laguerre-Gaussian (LG) laser beam. LG laser beam has an optical vortex in its center. The optical vortex is a point of zero intensity. The phase of the light field circulates around this zero intensity point. Integrating the phase of the light field around a path enclosing the vortex yields an integer multiple of 2π. The integer corresponds to the order of the optical vortex. The LG laser beam has the following form at any plane along the propagation axis z

$$\psi \propto r^{|m|} e^{im\phi} e^{-r^2} \tag{2}$$

where r and Φ are the polar coordinate with the optical vortex at the center, m is the order of the optical vortex. We used the method described in reference 7 to generate the computer generated hologram (CGH) for the optical vortex. When we shined a Gassian beam of fundamental mode onto the CGH, at the different diffraction orders of the CGH there were corresponding orders of optical vortices.

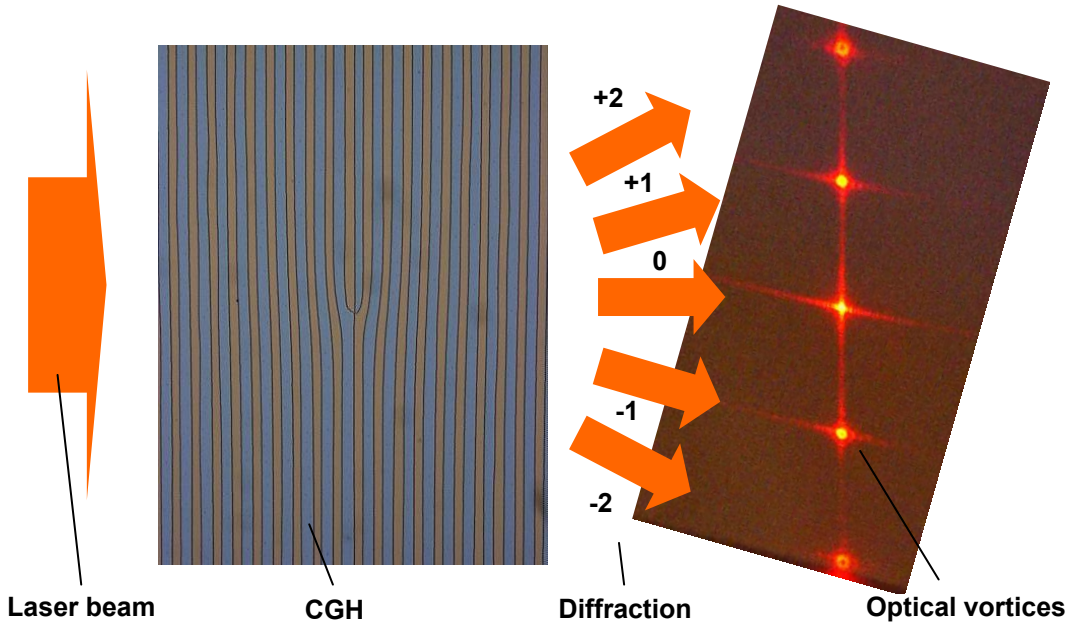

Figure 6: Generation of optical vortices by CGH

Again we used a Thorlabs C220TM-B lens to focus the first order optical vortex onto the double axes device. Then we raster-scanned our device across the first optical vortex at the focal plane of the lens, Figure 7 (a). Figure 7 (b) shows the intensity profile of the optical vortex. The donut shape beam profile is consistent with the expectation. Figure 7 (c) and (d) show the differential phases of the first optical vortex in X and Y directions respectively.

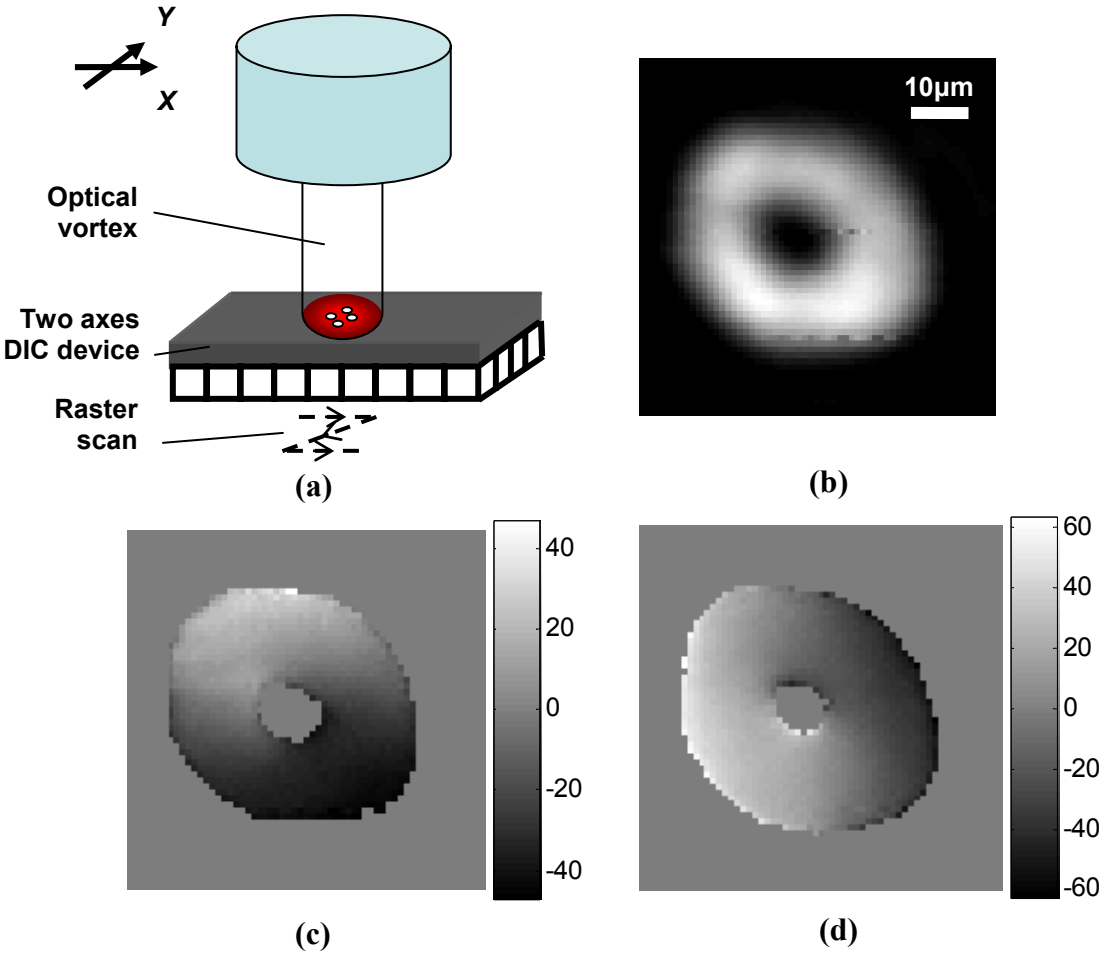

Figure 7: (a) Double axes beam profiling setup for an optical vortex. The intensity profile (b), the differential phases of the first order optical vortex in X (c) and Y (d) directions respectively.

If we combine the differential phases in X and Y directions together, the 2D differential phase vector field of the first order optical vortex can be established. In Figure 8, the phase circulating of the optical vortex is observed in the 2D differential phase vector field of the first order optical vortex recorded by our dual axes DIC device. As far as we know, it's the first time to record the 2D differential phase vector field of the optical vortex directly and quantitively with 1μm lateral resolution.

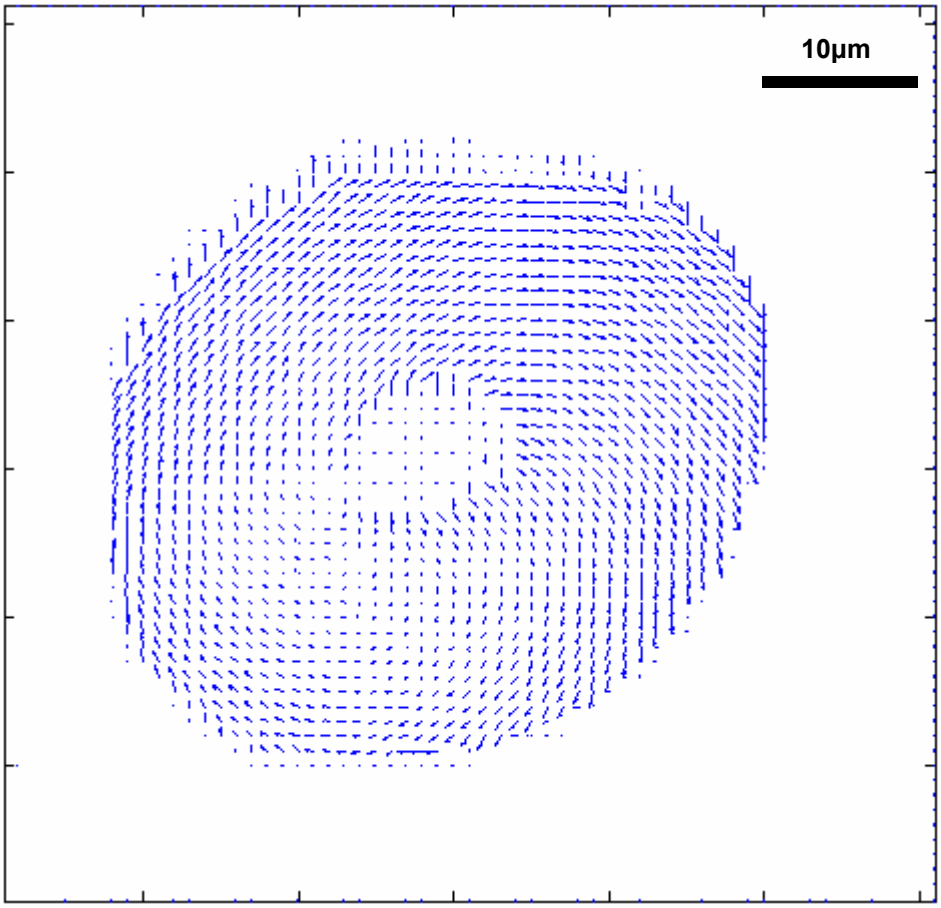

Figure 8: 2D differential phase vector field of the first order optical vortex.

5. Conclusion and future work

In this paper, we have presented the world's smallest DIC phase imaging device based on Young's interference. It provides linear and disentangled differential phase and intensity images simultaneously. Furthermore, it is simple, free of bulky optical elements and compatible to the planar micro fabrication process.

It also can be easily adapted as a DIC phase imaging sensor for OFM. One way of building DIC OFM with this device is simply that instead of using a linear array of single nano apertures in conventional OFM we could use four nano apertures pairs. As in the conventional OFM, when a cell or microorganism flow through the microfluidic channel, each four nano apertures pair will record a line trace of the transmission DIC and intensity images of the sample. By reconstructing the data appropriately, we will get these two transmission DIC and intensity images simultaneously and separately. With this sufficient knowledge of the transmission wave front of the sample, we should be able to reconstruct the structure of the sample in any given plane numerically. This will bring DIC and even volumetric imaging capability to the OFM family.

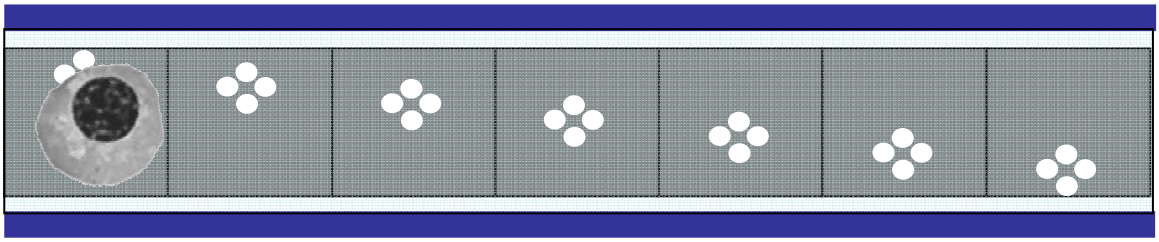

Figure 9: A way to build DIC OFM.

6. Acknowledgement

We are grateful for the generous help from Professor Axel Scherer. The assistance from Caltech Watson cleanroom is well appreciated. This project is funded by DARPA's center for optofluidic integration and Coulter Foundation Career Award.

REFERENCES

[1] D. Psaltis, S. Quake, and C. Yang, Developing optofluidic technology through the fusion of microfluidics and optics, Nature, vol. 442, 381-386, 2006.
[2] X. Heng, D. Erickson, L. R. Baugh, Z. Yaqoob, P. W. Sternberg, D. Psaltis, and C. Yang. Optofluidic microscopy: A method for implementing high resolution optical microscope on a chip, Lab on a Chip, vol. 6, 1274-1276, 2006.
[3] X. Cui, X. Heng, J. Wu, Z. Yaqoob, A. Scherer, D. Psaltis, and C. Yang. Slanted Hole Array Beam Profiler (SHArP) - A high resolution on-chip beam profiler based on a linear aperture array, Optics Letters, vol. 31, 3161-3163, 2006.

[4]X. Heng , E. Hsiao , D. Psaltis and C. Yang , A high resolution OptoFluidic Microscope with optical tweezer actuation, Photonics West, 2007
[5] R. V. Shack and B. C. Platt, Production and use of lenticular Hartmann screen, in Programme 1971 Spring Meeting Opt. Soc. Amer.,Washington, DC, 1971.
[6] C. J. Cogswell, C. J. R. Sheppard, Confocal differential interference contrast (DIC) microscopy: including a theoretical analysis of conventional and cofocal DIC imaging, Journal of Microscopy, vol. 165, 81-101, 1992.
[7] Z. S. Sacks, D. Rozas, and G. A. Swartzlander, Jr. Holographic formation of optical-vortex filaments J. Opt. Soc. Am. B, vol. 15, 2226-2234, 1998.